

## Development of micro milling force model and cutting parameter optimization

Shih-ming WANG, Da-fun CHEN, Min-chang JANG, Shambaljamts TSOOJ

Department of Mechanical Engineering, Chung Yuan Christian University, Taoyuan County 32023

Received 21 May 2012; accepted 1 November 2012

**Abstract:** Taking the minimum chip thickness effect, cutter deflection, and spindle run-out into account, a micro milling force model and a method to determine the optimal micro milling parameters were developed. The micro milling force model was derived as a function of the cutting coefficients and the instantaneous projected cutting area that was determined based on the machining parameters and the rotation trajectory of the cutter edges. When an allowable micro cutter deflection is defined, the maximum allowable cutting force can be determined. The optimal machining parameters can then be computed based on the cutting force model for better machining efficiency and accuracy. To verify the proposed cutting force model and the method to determine the optimal cutting parameters, micro-milling experiments were conducted, and the results show the feasibility and effectiveness of the model and method.

**Key words:** micro-milling; cutting force; spindle run out; cutter deflection; optimal parameter

### 1 Introduction

Miniaturization has become the design trend of high-tech products. Although MEMS technology has been used in many manufacturing applications, because of its limits on producing complex 3D shapes for variety of materials, many researchers have paid much attention to the development of non-MEMS micro manufacturing technology. Because micro milling can be directly used for making the micro parts or used to make the micro molds/dies for other micro manufacturing process such as micro injection and micro forging, it is recognized as a key technology in the non-MEMS micro manufacturing field.

For regular milling, TLUSTY and MANEIL [1] first proposed that the tangential cutting force is proportional to the cutting area that is function of chip thickness. Besides, the radial cutting force is also proportional to the tangential cutting force. Guk et al. [2] utilized finite element method to build the model for cutting dynamics. In the method, eccentric motion of tool was taken into account, and coordinate transformation was employed to identify the edge elements. When more information about tool material and tool structure was provided, the model can accurately explain the cutting dynamics. It can reach accuracy of 90% for the

prediction of cutting force.

However, the dynamic behavior of micro milling is different from regular milling. VOGLER et al [3] developed a cutting force model for composite materials. Basically the model was function of cutting area with material coefficient. According to the experimental results with pure copper, RAHMAN et al [4] discovered that micro milling and regular milling would have same shape of chips but in different sizes. The cutter life is dependent on helix angle of cutter, and the tangential cutting force is proportional to the axial cutting force. BISSACCO et al [5] proved that the eccentric deviation of a cutter has influence on cutting force, and it should be taken into account for cutting force prediction. LIU et al [6] found that the minimum chip thickness was smaller than radius of the micro cutter tip, and it was influenced by the cutting force, surface roughness of cutter, and stability of cutting etc. ZAMAN et al [7] proposed a 3D micro milling force model. The model determined the cutting force by calculating the projected cutting area. However, since it can only approximately calculate the projected area and did not take the minimum chip thickness, cutter deflection, and spindle run out into account, errors existed in the cutting force prediction.

With use of micro cutters, micro milling is expected to provide ultra-precision machining for complex 3D micro feature/contour. However, because the micro cutter

is too thin to have good stiffness, cutting forces will cause cutter vibration and cutter deflections that deteriorate the machining accuracy or even break the cutter. Thus, the cutting force should be properly controlled in a micro milling process. Although small depth of cut at high spindle speed is usually planned for micro milling, the minimum chip thickness condition should be considered. In addition, because spindle run-out could result in changes in depth of cut and cutting forces, it should also be taken into account for cutting force prediction.

In this study, considering the effect of minimum chip thickness, rake angle of cutter, cutter deflection, and spindle run-out, a new model for determining micro milling forces was proposed. The model that can determine the micro-milling force using the same set of cutting coefficients for the applications with different axial depths of cut was addressed. The micro milling force model was derived as a function of the cutting coefficients and the instantaneous projected cutting area. Thus, the method to calculate the instantaneous cutting area projected to  $x$ - $y$  plane based on the machining parameters and the rotation trajectory of the cutter edges was also developed in this study. Furthermore, based on the cutting force model, a method to determine the optimal machining parameters was proposed. When an allowable micro cutter deflection was given, the maximum allowable cutting force was estimated by CAE analysis. The optimal machining parameters could then be determined based on the cutting force model for better machining efficiency. Finally, verification experiments were conducted, and the experimental results were discussed.

### 2 Cutting force model

The total cutting force can be divided into tangential cutting force, radial cutting, and axial cutting force. The direction of the tangential cutting force ( $F_t$ ) depends on the instantaneous rotation trajectory of the cutter. The radial cutting force ( $F_r$ ) pushes the cutting edge away from the workpiece in the  $x$ -direction. Meanwhile, the axial cutting force ( $F_z$ ) is acting in the  $z$ -direction. The micro milling cutting forces for a fixed axial depth of cut model can be solved (Zaman et al [7]) as

$$\text{Tangential cutting force: } F_{ti} = K_m + A_{pi} \tag{1}$$

$$\text{Radial cutting force: } F_{ri} = qF_{ti} + F_{elastic}A_{pi} \tag{2}$$

$$\text{Axial cutting force: } F_{zi} = -F_{ai} = -F_{ti} \sin \psi \tag{3}$$

where  $i$  represents the instantaneous cutting point on the cutting trajectory;  $A_{pi}$  represents the instantaneous cutting area shown in Fig. 1;  $q$  represents the proportional constant;  $\psi$  represents the helix angle of the cutter;  $K_m$

represents the cutting coefficients;  $F_{elastic}$  represents the force due to elastic deformation. Because the elastic strain occurring in the cutting experiment is very small, it is temporarily neglected here. Those coefficients can be determined based on a micro-milling experiment with a fixed axial depth of cut. The details of the procedure will be addressed later.

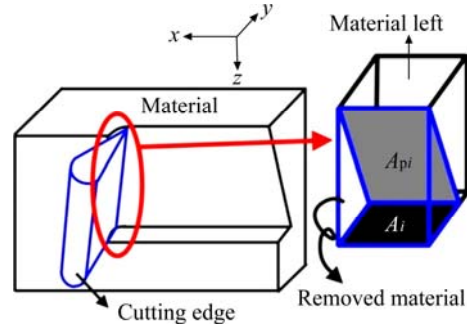


Fig. 1 Illustration of projected cutting area

The instantaneous cutting area  $A_{pi}$  can be solved when the projected cutting area  $A_i$  that is the projection of  $A_{pi}$  on  $x$ - $y$  plane (Fig.1) is known. The relationship between  $A_i$  and  $A_{pi}$  is

$$A_{pi} = \frac{A_i}{\sin \psi} \tag{4}$$

When the projected cutting area  $A_i$  is known, it can be substituted into Eq. (4) to solve  $A_{pi}$ ,  $F_{ti}$ ,  $F_{ri}$ , and  $F_{ai}$  can, then, be solved according to Eqs. (1)–(3).

The cutting forces solved by Eqs. (1), (2), and (3) can then be converted into the cutting forces in the  $x$ -,  $y$ -, and  $z$ -direction (as shown in Fig. 2). In Fig. 2,  $T1$  and  $T2$  are respectively the continuous rotation trajectory of the cutter when the center of the cutter is at  $O1$  and  $O2$ , and  $\phi_i$  represents the instantaneous rotation angle of the cutter.  $A$  and  $B$  are respectively the initial cutting points of trajectories  $T2$  and  $T1$ . Point  $C$  is the intersection of  $T1$  and  $T2$ . The cutting force in  $x$ -,  $y$ - and  $z$ - direction can be

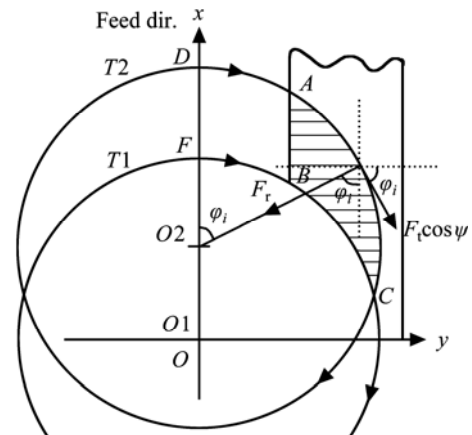


Fig. 2 Cutting trajectories on  $x$ - $y$  plane

expressed as

$$F_{xi}=(F_{ti} \cos \psi) \sin \varphi_i-F_{ri} \cos \varphi_i \quad (5)$$

$$F_{yi}=(F_{ti} \cos \psi) \sin \varphi_i-F_{ri} \cos \varphi_i \quad (6)$$

$$F_{zi}=-F_{ai}=-F_{ti} \sin \varphi_i \quad (7)$$

### 3 Determination of projected cutting area

To use Eqs. (1)–(3) to determine the cutting forces, the projected cutting area needs to be solved first. Area  $ABC$  ( $A_i$ ) shown in Fig. 2 is the projected cutting area when the cutting edge moves along the planned  $T2$ . When the material is cut, both elastic deformation and plastic deformation occur. The elastic deformation occurs within the region where the chip thickness is smaller than the minimum chip thickness, and the plastic deformation occurs in the region where the chip thickness is greater than the minimum chip thickness. The true projected cutting area in which the material will be really cut should equal area  $ABC$  (in Fig. 2) minus the elastic deformation area. The white area shown in Fig. 3 represents the true projected cutting area, and the red region is the elastic-deformation area. According to the model proposed by SEONG et al [8], the minimum chip thickness  $t_m$  can be expressed as

$$t_m=r\left[1-\cos\left(\frac{\pi}{4}-\frac{\beta}{2}\right)\right] \quad (8)$$

where  $r$  is the radius of the cutter, and  $\beta$  represents the friction angle between the cutter and workpiece which is also equals the shear angle  $\Phi$  in Fig. 4. According to Ref. [9], the shear angle can be determined as follows:

$$\Phi=\tan^{-1}\left(\frac{r \cos \alpha}{1-r \sin \alpha}\right) \quad (9)$$

$$r=\frac{t}{t_c} \quad (10)$$

where  $t$  is the depth of cut, and  $t_c$  is chip thickness.

Based on Eqs. (8), (9) and (10), the minimum chip thickness can be solved and used to calculate the true projected cutting area. By considering the minimum chip thickness the true projected cutting area (shown in Fig. 2) can be calculated using the rectangular integral. The calculation is independent of the instantaneous location of the cutting edge. According to the location of the cutter tip, the true projected cutting area was distinguished into three cases.

Case 1: Area ( $AA''B'$ ) (Fig. 5) when  $\varphi_A < \varphi_i \leq \varphi_B$

In Fig. 3,  $A$  and  $A'$  are the cutting points on  $T2$ ;  $B$  and  $B'$  are respectively the first cutting points on trajectories  $T1$  and  $T2$ ; is  $L0$  the line connecting the first cutting point  $A$  and  $O2$ ; is  $L1$  the line connecting the first cutting point  $B$  and  $O2$ ;  $L$  represents the line connecting

the instant cutting point  $A''$  on  $T2$  and  $O2$ ;  $\varphi_i$  represents the instantaneous cutting angle between  $L$  and the  $x$ -axis; and  $y1$  is the edge of the workpiece parallel to the  $x$ -axis.

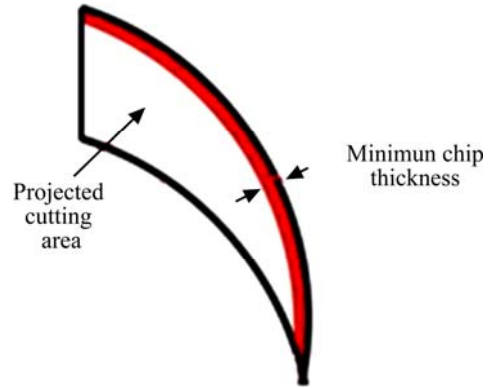


Fig. 3 Schematic diagram of elastic-deformation region

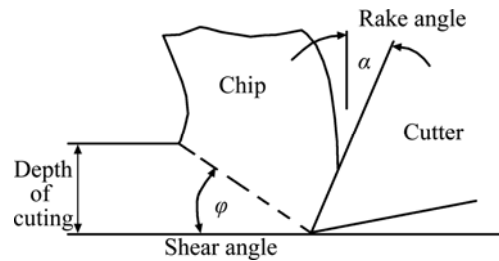


Fig. 4 Schematic diagram of shear angle and rake angle

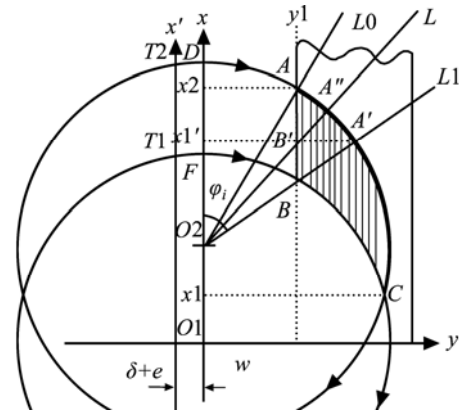


Fig. 5 Projected cutting area for  $\varphi_A < \varphi_i \leq \varphi_B$

Considering the effect of minimum chip thickness, the equation of  $T2$  is

$$(x-x_{O2})^2+y_2^2=r_c \quad (11)$$

$$r_c=r-t_m \quad (12)$$

For  $T2$ , the center of cutter locates at  $(vt, 0)$ .  $v$  is the cutting federate, and  $t$  is the machining time. Therefore,  $x_{O2}=vt=a_2$ . If the tip of the cutting edge locates between  $A$  and  $A'$ , the coordinates of any point on  $T2$  are  $(r_c \cos \varphi_i+vt, r_c \sin \varphi_i)$ . The equation of  $L$  is  $[\tan(90^\circ-\varphi_i)]y-x=0$  (13)

Because the center of cutter is at (0, 0), the equation of T1 can be expressed as  $x^2+y^2=r_e$ , where  $y=w$  represents the distance between the center of the cutter and the edge of workpiece. Further,

$$x = \pm\sqrt{r_e^2 - w^2} \tag{14}$$

According to Eq. (16), the coordinates of B are obtained as  $(\sqrt{r_e^2 - w^2}, w)$  and

$$\varphi_B = \tan^{-1}\left(\frac{w}{\sqrt{r_e^2 - w^2 - vt}}\right),$$

$$\varphi_A = \sin^{-1}\left(\frac{w}{r_e}\right) \tag{15}$$

Finally, area  $AA''B'$  can be expressed as

$$A_{AA'B'} = \int_w^{r_e \sin \varphi_i} (T2 - L) dy = \int_w^{r_e \sin \varphi_i} [a_2 + \sqrt{r_e^2 - y^2} - (\cot \varphi_i) y] dy \tag{16}$$

If the cutter deflection ( $\delta$ ) and spindle run-out ( $e$ ) exist, the  $x$  axis in Fig. 5 will deviate to  $x'$  axis. That is, the center of the cutter will deviate from its nominal position for  $(\delta+e)$ , and the lower limit in Eq. (16) becomes  $w+\delta+e$ . The area  $AA''B'$  can be solved as

$$A_{AA'B'} = vt(r_e \sin \varphi_i - w - \delta - e) + \frac{r_e^2}{2} \sin^{-1}\left(\frac{w - \delta - e}{r_e}\right) - \frac{1}{2}(w + \delta + e)\sqrt{r_e^2 - (w + \delta + e)^2} + \frac{1}{2}(w + \delta + e)^2 \cos \varphi_i \tag{17}$$

Case 2: Area  $AA''C''B$  (Fig. 6) when  $\varphi_B < \varphi_i < 90^\circ$

When  $\varphi_i = 90^\circ$ ,  $L$  is normal to the  $x$ -axis like  $L2$ ,  $A_{AA''C''B} = A_{AA''D''} - A_{BC''D''}$ . Taking cutter deflection ( $\delta$ ) and spindle run-out ( $e$ ) into account, area  $(AA''D')$  can be solved as

$$A_{AA''D'} = \int_{w+\delta+e}^{r_e \sin \varphi_i} (T2 - L) dy = vt(r_e \sin \varphi_i - w - \delta - e) + \frac{r_e^2}{2} \varphi_i - \frac{r_e^2}{2} \sin^{-1}\left(\frac{w + \delta + e}{r_e}\right) - \frac{1}{2}(w + \delta + e) \cdot \sqrt{r_e^2 - (w + \delta + e)^2} + \frac{1}{2}(w + \delta + e)^2 \cot \varphi_i \tag{18}$$

And area  $BC''D'$  can be solved as

$$A_{BC''D'} = \int_{w+\delta+e}^{x_e \sin \varphi_i} (T1 - L) dy = \int_{w+\delta+e}^{x_e \sin \varphi_i} \left(\sqrt{r_e^2 - y^2}\right) dy - \int_{w+\delta+e}^{x_e \sin \varphi_i} (\cot \varphi_i) y dy + \frac{r_e^2}{2} \left[ \frac{x_e \sin \varphi_i \sqrt{r_e^2 - (x_e \sin \varphi_i)^2}}{r_e^2} \right]$$

$$\left. \frac{(w + \delta + e)\sqrt{r_e^2 - (w + \delta + e)^2}}{r_e^2} \right] - \frac{1}{2}(\cot \varphi_i)(x_e \sin \varphi_i)^2 - (w + \delta + e)^2 \tag{19}$$

Finally, area  $AA''C''B$  is obtained as

$$A_{AA''C''B} = vt(r_e \sin \varphi_i - w - \delta - e) + \frac{r_e^2}{2} \varphi_i - \frac{r_e x_e}{2} \varphi_i - \frac{1}{2} x_e \sin \varphi_i \sqrt{r_e^2 - (x_e \sin \varphi_i)^2} - \frac{1}{2} x_e \cot \varphi_i \left(\frac{1}{2} x_e^2 \sin^2 \varphi_i\right) \tag{20}$$

Case 3: Area  $AA''C''B$  (Fig. 7) when  $90^\circ \leq \varphi_i \leq \varphi_c$

Following similar procedures, it is noted that

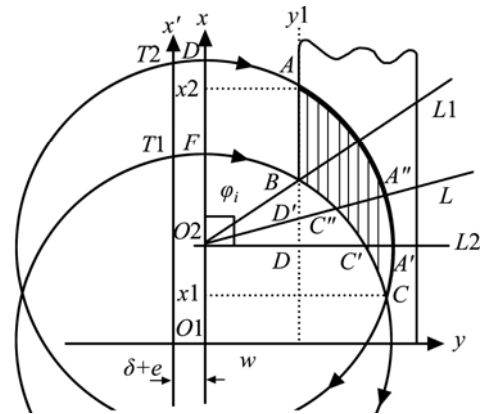


Fig. 6 Projected area when  $\varphi_B < \varphi_i < 90^\circ$

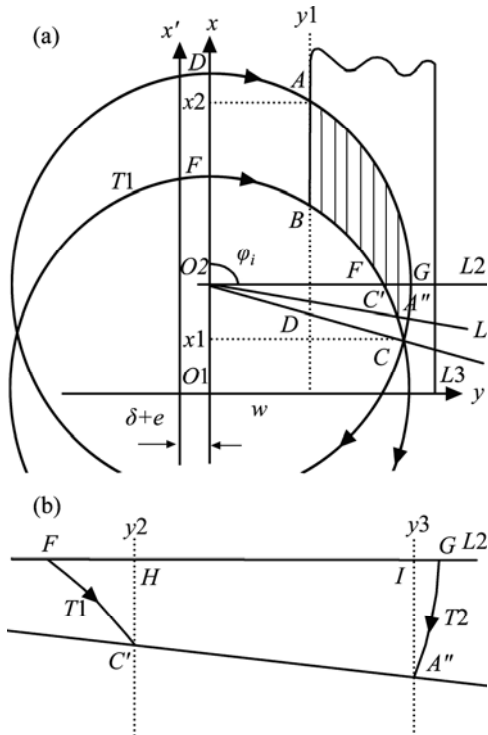


Fig. 7 Projected cutting area when  $90^\circ \leq \varphi_i \leq \varphi_c$ : (a) Projected area when  $90^\circ \leq \varphi_i \leq \varphi_c$ ; (b) Enlarged figure of area  $FGA''C'$

$$S_{AA''CB} = S_{AGFB} + S_{FGA''C'}$$

Area  $AFGB$  can be solved by Eq. (20). As shown in Fig. 7(b), area  $FGA''C'$  is the sum of areas  $FHC'$ ,  $HIA''C'$ , and  $IGA''$ . Area  $FHC'$  can be calculated as follows:

$$\begin{aligned} A_{FHC'} &= \int_{\sqrt{r_e^2 - (vt)^2}}^{r_e \sin \varphi_i} (L2 - T1) dy = \\ & (vt)(x_c \sin \varphi_i) - \frac{vt}{2} \sqrt{r_e^2 - (vt)^2} - \\ & \frac{r_e^2}{2} \left[ \left( \frac{x_c \varphi_i}{r_e} \right) - \sin^{-1} \left( \frac{\sqrt{r_e^2 - (vt)^2}}{r_e} \right) \right] - \\ & \frac{1}{2} x_c \sin \varphi_i \sqrt{r_e^2 - (x_c \sin \varphi_i)^2} \end{aligned} \quad (21)$$

Area ( $HIA''C'$ ) can be determined as

$$\begin{aligned} A_{HIA''C'} &= \int_{x_c \sin \varphi_i}^{r \sin \varphi_i} (L2 - T1) dy = \int [vt - (\cot \varphi_i) y] dy = \\ & (vt)(r_e - x_c) \sin \varphi_i - \frac{1}{2} (\cos \varphi_i)(r_e^2 - x_c^2)(\sin \varphi_i) \end{aligned} \quad (22)$$

Area  $IGA''$  can be determined as follows:

$$\begin{aligned} A_{IGA''} &= \int_{r_e \cos \varphi_i + vt}^{vt} (T2 - Y1) dx = \\ & \int_{r_e \cos \varphi_i + vt}^{vt} \left[ \sqrt{r_e^2 - (x - vt)^2} - r \sin \varphi_i \right] dx = \\ & \frac{r_e^2}{2} [(\sin \varphi_i)(\cos \varphi_i) + \tan^{-1}(-\cos \varphi_i)] \end{aligned} \quad (23)$$

According to Eqs. (23)–(25), Area  $FGA''C'$  can be obtained as

$$\begin{aligned} A_{FGA''C'} &= vt(r_e - w - \delta - e) + \frac{\pi r}{4}(r_e - x_c) - \\ & \frac{1}{2} x_c \sqrt{r_e^2 - x_c^2} - \left( \frac{vt}{2} \right) \sqrt{r_e^2 - (vt)^2} - \\ & \frac{r_e^2}{2} \left[ \left( \frac{x_c}{r_e} \right) \varphi_i - \sin^{-1} \frac{\sqrt{r_e^2 - (vt)^2}}{r_e} \right] - \\ & \frac{1}{2} x_c \sin \varphi_i \sqrt{r_e^2 - (x_c \sin \varphi_i)^2} + (vt)r_e \sin \varphi_i \end{aligned} \quad (24)$$

Finally, Area  $AA''CB$  can be obtained as the sum of Area  $AGFB$  (Eq. (20)) and area  $FGA''C'$  (Eq. (24)).

#### 4 Relationship between axial depth of cut and projected cutting area

The cutting force model is a function of the instantaneous cutting area calculated based on the projected cutting area. When the axial depth of cut is

smaller than the spiral pitch of the flute, the projected cutting area is proportional to the axial depth of cut. When the axial depth of cut is greater than the spiral pitch of the flute, the projected cutting area will remain constant. However, the larger axial depth of cut is taken, the larger cutting force will be generated. Figure 8 shows the relationships between axial depth of cut, the helix angle  $\psi$ , and the spiral pitch ( $d = L \tan \psi$ ). Thus, accumulating projected cutting area should be calculated based on the axial depth of cut, and used for Eq. (4). When the axial depth of cut is set as  $H$ , Eq. (4) becomes

$$A_{pi} = \frac{A_i}{\sin \psi} \times \frac{H}{L \tan \psi} \quad (25)$$

Where  $L$  is the circumference of the micro cutter; and  $\psi$  is the helix angle of the cutter.

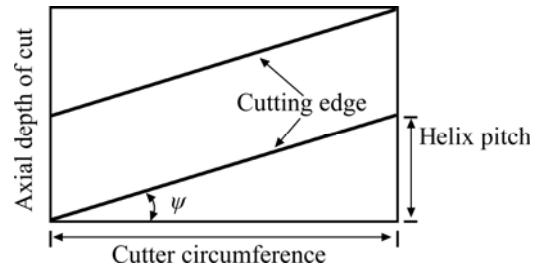


Fig. 8 Relationship between axial depth of cut, helix angle and spiral pitch

#### 5 Determination of $K_m$ and $q$

Coefficients  $K_m$  and  $q$  should be determined by practical micro-milling experiments. First, the  $z$ -direction cutting force  $F_{zi}$  should be measured from the experiment. Subsequently, the tangential cutting force  $F_{ti}$  is solved based on Eq. (7). Then,  $K_m$  can be calculated based on Eq. (1) with the known cutting area  $A_{pi}$ . On the other hand, when  $F_{yi}$  is measured, the radial cutting force  $F_{ri}$  can, then, be solved from Eq. (6). By substituting  $F_{ri}$  into Eq. (2), coefficient  $q$  can be determined.

#### 6 Determination of cutter deflection

A 2-flute micro milling cutter was used in this experiment. With the assumption of the cross section area of each flute is equal to one quarter of the area of an ellipse, according to the principle of mechanics of materials the moment of inertia of the cutter was derived and used to compute the cutter deflection caused by cutting forces. The results were compared with the CAE simulation made by ANSYS software. From Fig. 9, it can be seen that the results made by the two methods are very similar and consistent. The relationship curve between cutter deflection and cutting force (Fig. 9) was

built and used for the estimation of the maximum allowable cutting force when an allowable cutter deflection was given.

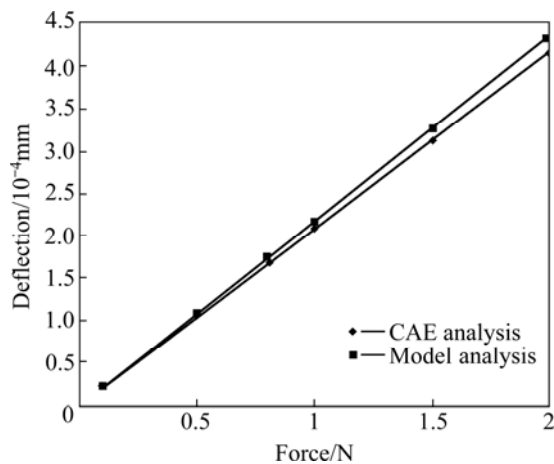


Fig. 9 Cutter deflection vs cutting force

## 7 Determination of optimal cutting parameters

Improper machining parameters could cause unbearable cutting forces and vibrations deteriorating the machining accuracy or break the micro cutter. To ensure a good machining performance, the optimal machining parameter could be determined based on the maximum allowable cutter deflection. The maximum allowable cutter deflection can be obtained through model analysis or CAE analysis as mentioned in Section 4. When the maximum allowable cutter deflection is given, the maximum allowable cutting forces can be determined based on the relationship between cutter deflection and cutting force (as shown in Fig. 9). According to the maximum allowable cutting force, the associated projected cutting area can be determined based on the proposed cutting force model. Since the projected cutting area is function of feedrate and the cutting force is proportional to the axial depth of cut, the maximum feedrate and axial depth of cut of a micro milling can be determined by the equations derived in Sections 3 and 4.

## 8 Experiments

Micro milling experiments were conducted on a micro machine tool designed by our lab. A 3-direction force sensor was used. Specifications of equipments and instruments used are listed in Table 1. A 2-flute micro end-mill with 0.5 mm in diameter was used to cut copper. The helix angle and radius of the edge tip of the cutter were 45° and 4.23 μm, respectively. The cutting parameters used for determination of  $K_m$  and  $q$  are follows: axial depth of cut (ADC) is 0.3 mm, radial depth of cut (RDC) is 0.3 mm, spindle speed is 130000 r/min, and federate is 30 mm/min. The measured average

maximum cutting forces in  $x$ -,  $y$ - and  $z$ -direction were 1.45, 1.5, and 49 N, respectively. By substituting the forces into Eqs. (5)–(7), the cutting forces  $F_{t_i}$ ,  $F_{r_i}$ , and  $F_{a_i}$  were solved and substituted into Eqs. (1)–(3). The cutting coefficients were then obtained as  $K_m$  of 112.65755 kN/mm<sup>2</sup> and  $q$  of 2.89. Two micro displacement sensors were set up in  $x$ - and  $y$ -direction on the micro machine tool to measure the run-out of the spindle. With the same cutting parameters but ADC is 0.4 mm, verification cutting experiment was conducted. Figure 11 shows the actual cutting forces and model-predicted cutting forces in  $x$ -,  $y$ - and  $z$ -direction. It can be seen that the predicted cutting forces has very similar periodic variation as the actual cutting forces did. The prediction accuracy of the force model is 80%–88% (Table 2). To verify the reliability of the model, another cutting experiment with different cutting parameters (ADC of 0.3 mm, RDC of 0.1 mm, spindle speed of 130000 r/min, federate of 30 mm/min.), but same cutting coefficients was conducted. Figure 12 shows the actual cutting forces and model-calculated cutting forces in  $x$ -,  $y$ - and  $z$ -direction. Table 3 shows the comparison of the actual cutting forces and model-predicted cutting forces. It is noted that prediction accuracy of the model still remains at 83%–90%.

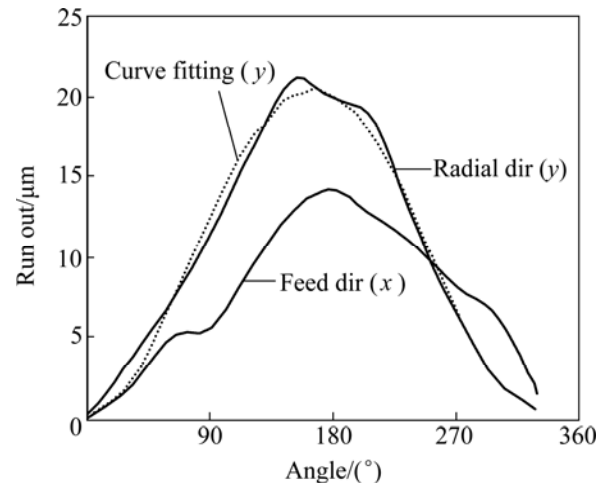
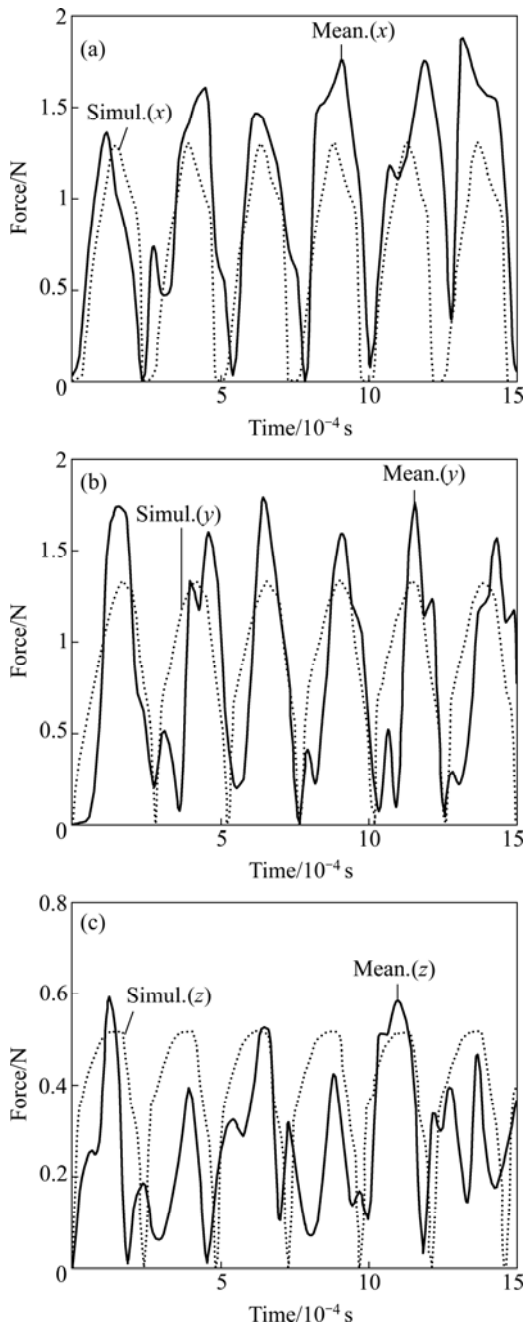


Fig. 10 Measured spindle run-out

Table 1 Equipments and instruments

Spindle	Measurement Instrument	$x$ - $y$ stage
NSK HTS1501S-M2040 (150000 r/min)	3-direction force sensor: PCB 260A01	Frequency analyzer: Portable PULSE-3560C Driven by liner motors; resolution: 1 μm

For determination of optimal cutting parameters, a 2-flute micro end-mill with 0.7 mm in diameter was used to cut copper for the optimization experiment, and the maximum allowable cutter deflection of 200 nm was



**Fig. 11** Actual and predicted cutting forces in the 1st experiment: (a) *x*-direction; (b) *y*-direction and (c) *z*-direction

**Table 2** Comparison of actual and predicted forces in 1st experiment

Axis	Measured force/N	Predicted force/N	Prediction accuracy/%
<i>x</i>	1.620	1.30	80.2
<i>y</i>	1.688	1.33	79.2
<i>z</i>	0.452	0.51	88.6

chosen. The cutting parameters, ADC of 0.4 mm, RDC of 0.3 mm, spindle speed of 130000 r/min, were set. The optimal federate is unknown, but it will be determined

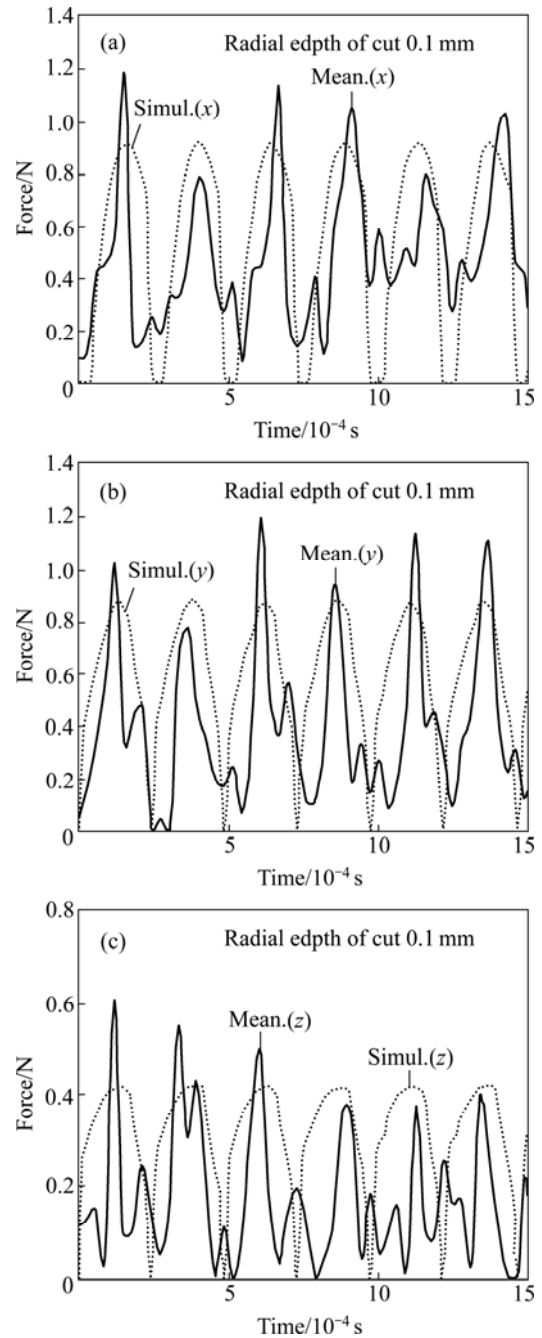


**Fig. 12** Actual and predicted cutting forces in the 2nd experiment: (a) *x*-direction; (b) *y*-direction and (c) *z*-direction

with the proposed method.

According to the CAE analysis made by ANSYS software, the allowable maximum radial cutting force  $F_{ri}$  was 0.95 N. After substituting  $F_{ri}$ ,  $K_m=112657.55$ , and  $q=2.89$ , into Eqs. (1), (2), and (4), the recommended allowable maximum federate was solved as 0.33 mm/s. By using the recommended feedrate, a micro milling experiment was conducted. Figure 13 shows the comparison of the actual cutting forces and predicted cutting forces in *x*-, *y*-, and *z*- direction. It is noted that the actual cutting forces are very close to the predicted cutting forces in both magnitude and trend. This means

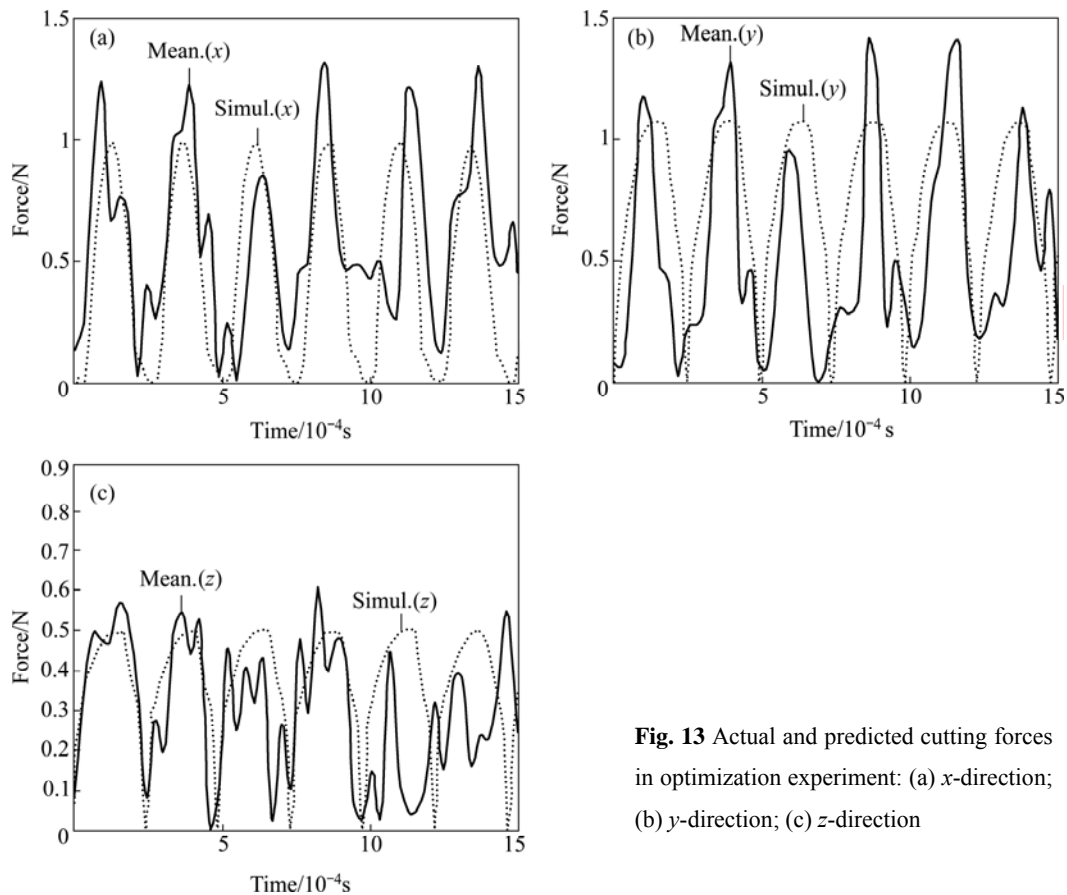


**Fig. 13** Actual and predicted cutting forces in optimization experiment: (a)  $x$ -direction; (b)  $y$ -direction; (c)  $z$ -direction

**Table 3** Comparison of actual and predicted forces in the 2nd experiment

Axis	Measured force/N	Predicted force/N	Prediction accuracy/%
$x$	0.900	0.99	90.9
$y$	0.875	1.05	82.9
$z$	0.41	0.47	87.2

that the optimal cutting parameters can be solved to control the cutting forces so that the cutter deflection can be confined for better machining accuracy or cutter life.

## 9 Conclusions

A new cutting force model that can predict the cutting forces for micro milling process was proposed. The model can be used to predict cutting force with different cutting parameters without changing the coefficients. Based on the model, a method that can design optimal cutting parameters for allowable maximum cutter deflection control was also developed. Experimental results show the feasibility and effectiveness of the proposed force model and the method.

## References

- [1] TLUSTY J, MANEIL P. Dynamics of cutting force in end milling [J]. *Annals of CIRP*, 1975, 24(1): 21–25.
- [2] JUN B G, DEVOR R E, KAPOOR S G. Investigation of the dynamics of micro-end milling, Part I: Model development [J]. *Journal of Manufacturing Science and Engineering*, 2006, 128: 893–900.
- [3] VOGLER M P, DEVOR R E, KAPOOR S G. Microstructure-level force prediction model for micro-milling of multi-phase materials [J]. *Trans of the ASME*, 2003, 125: 202–209.
- [4] RAHMAN M, SENTHIL KUMAR A, PRAKASH J R S. Micro milling of pure copper [J]. *Journal of Materials Processing Technology*, 2001, 116: 39–43.
- [5] BISSACCO G, HANSEN H N, SLUNSKY J. Modelling the cutting edge radius size effect for force prediction in micro milling [J]. *Manufacturing Technology*, 2008, 57: 113–116.
- [6] LIU X, DEVOR R E, KAPOOR S G. An analytical model for the prediction of minimum chip thickness in micromachining [J]. *Journal of Manufacturing Science and Engineering*, 2006, 128(2): 474–481.
- [7] ZAMAN M T, KUMAR A S, RAHMAN M, SREERAM S. A three-dimensional analytical cutting force model for micro end milling operation [J]. *International Journal of Machine Tools & Manufacture*, 2005, 46: 353–336.
- [8] SON S M, LIM H S, AHN J H. Effects of the friction coefficient on the minimum cutting thickness in micro cutting [J]. *International Journal of Machine Tools & Manufacture*, 2005, 45: 529–535.
- [9] SHAW M C. *Metal cutting principles* [M]. Cambridge: Technology Press, 1996.